Int J Adv Manuf Technol (2011) 53:505–516
DOI 10.1007/s00170-010-2879-9

ORIGINAL ARTICLE

Friction-stir welding of AA 2198 butt joints: mechanical characterization of the process and of the welds through DOE analysis

Ciro Bitondo · Umberto Prisco · Antonino Squilace · Pasquale Buonadonna · Gennaro Dionoro

Received: 9 June 2010 / Accepted: 28 July 2010 / Published online: 15 August 2010

Abstract In this study, rolled plates of AA 2198 T3 aluminium alloy are friction-stir welded in butt configuration varying two fundamental process parameters: rotational and welding speeds. Two sets of empirical models based on regression analysis are developed. The first one predicts the stationary values of the in-plane and downwards forging welding forces in dependence of the process parameters under investigation. The second one predicts the mechanical strength, in particular yield and tensile strength, of the friction-stir welded joints as function of the same parameters. For the development of the empirical models, two 3^2 full factorial designs are used: one having the stationary values of the welding forces and the other having the yield and tensile strength as observed responses, respectively. Statistical tools such as analysis of variance, F tests, Mallows' C_P, coefficient of determination etc. are used to build and to validate the developed models. By using the desirability function approach, the optimum process parameters to simultaneously obtain maximum possible yield and tensile strength are found within the investigated range. The developed models can be effectively used to predict the stationary forces and the mechanical proprieties of the joints at 95% confidence level.

C. Bitondo · U. Prisco (✉) · A. Squilace
Department of Materials and Production Engineering,
University of Naples Federico II,
Piazzale Tecchio,
Naples, Italy
e-mail: umberto.prisco@unina.it

P. Buonadonna · G. Dionoro
Department of Mechanical Engineering, University of Cagliari,
Piazza d'Armi,
Cagliari, Italy

Keywords AA 2198 · Friction-stir welding (FSW) · Rotational speed · Welding speed · FSW forces · Tensile strength · Design of experiments, desirability function (DF) approach

1 Introduction

Friction-stir welding (FSW) is a solid-state joining process in which the material that is being welded does not reach the melting point, in contrast to the fusion welding processes [1]. Due to the interesting features of FSW, lots of research activities have been carried out on different materials (aluminium alloys first of all, but also steel, titanium, magnesium, copper, polymers etc.) and on different weld geometries. In particular, FSW of AA 2198 aluminium alloy has gained wide use in the fabrication of lightweight structures requiring a high strength-to-weight ratio and good corrosion resistance [2].

In comparison with other welding techniques, FSW offers advantages for low residual stresses, low distortion and high joint strength [2, 3]. Nevertheless, during this process, the tool, with its rotational and welding speeds, exerts in-plane (horizontal) and downward (vertical) forging forces on the plates to be welded. These forces, joined to the thermal impact effect, may cause the deformation of the fixture and of the welded plates, as well as influence the tool wear. Hence, controlling the force is mandatory for FSW and can have strong consequences on the productivity and on the weld quality. Many significant benefits can be obtained keeping the welding forces at a definite level: optimization of fixturing, tool breakage prevention, tool life prediction, prediction of clamping forces, etc. Especially in robotic FSW, force controlling can be very helpful.

Table 1 Chemical composition (wt.%) of base AA 2198 aluminium alloy

	Si (%)	Fe (%)	Cu (%)	Mn (%)	Mg (%)	Cr (%)	Zn (%)	Zr (%)	Li (%)	Ag (%)
Min	–	–	2.90	–	0.25	–	–	0.04	0.80	0.10
Max	0.08	0.10	3.50	0.50	0.80	0.05	0.35	0.18	1.10	0.50

However, to build an efficient control technique for FSW, a well-founded force prediction model needs to be developed. The empirical model developed for the prediction of the welding forces can be further employed to get better insights into the mechanics of FSW, the correlation between the welding parameters and interdependence between the welding parameters and the weld quality. Development of FSW force models is not an easy task considering that it was proved that the clamping force contains static nonlinearities with respect to the tool rotational speed, longitudinal speed, tool plunge depth and the thermomechanical performance of the materials [3]. On the other side, it is also essential to have a complete control over the relevant process parameters to maximize the yield and tensile strength on which the quality of a weldment is based.

It has been proved by several researchers that efficient use of statistical design of experimental techniques allows development of an empirical methodology to incorporate a scientific approach in the FSW procedure [4–8]. Indeed, the design of experiments was used in several papers to conduct experimental campaigns for exploring the interdependence of process parameters, and to develop empirical models for the prediction of tensile strength of friction-stir welded joints.

For instance, using the design of experiments concept, response surface method and the Hooke and Jeeves algorithm, Elangovan et al. [6] developed a empirical model to predict the tensile strength of friction-stir welded AA 6061 aluminium alloy joints and optimized the FSW process parameters to attain maximum tensile strength. The model was developed by incorporating welding parameters and tool profiles and by using statistical tools such as design of experiments and regression analysis. Balasubramanian [7] established an empirical relationships to predict the FSW process parameters, in particular, tool rotational speed and welding speed, to fabricate defect free joints from the known base metal properties (yield strength, ductility and hardness) of aluminium alloys. Lakshminarayanan et al. [8], based on a three factors three-level central composite design with full replications, developed a response surface methodology to predict the tensile strength of friction-stir welded AA7039 aluminium alloy.

However, to the present authors' knowledge, sparse work has been carried out on prediction of both welding forces and mechanical proprieties of joints in FSW. Therefore, in this investigation an attempt is made to develop empirical models for the prediction of welding forces and mechanical strength (yield and tensile) of friction-stir welded joints. In addition, it is tried to optimize the FSW process parameters to attain maximum mechanical strength of friction-stir welded joints using the desirability function approach.

2 Experimental work

Rolled plates of 3.2 mm thickness AA 2198 T3 aluminium alloy were cut into the required size (200×100 mm) by power hacksaw cutting. The chemical composition and main mechanical properties of base alloy are listed in Tables 1 and 2.

The obtained plates were used to fabricate FSW joints in butt configuration (welds are 200 mm long), see Fig. 1a. The direction of welding was parallel to the rolling direction. Non-consumable tools, made of Cr-Mo steel, were used to fabricate the joints. Tool geometry is characterised by a shoulder radius of 12 mm and by an unthreaded cylindrical pin of 4 mm in diameter and 3 mm long. The forging action of the tool shoulder was enhanced by a forwards tool tilt angle of 2°. The plates were butt-welded using a five axes DMG CNC universal milling machine with a 0×600×600 (x/y/z) workspace. The machine was instrumented with a Kistler three-axis dynamic dynamometer for in-plane, *Fx*, and downwards forging, *Fz*, welding forces recording. For the force signal acquisition, the sampling rate was set at 10 Hz.

In all the experimental campaign, the welding process was divided in the following phases:

a) initial phase, during which the pin, moving along the *z*-axis, reaches the plates surfaces and penetrates into the material up to the shoulder;
b) plunging phase, during which the tool shoulder reaches the surface and is plunged into the joint line until the shoulder deepens 0.1 mm underneath the top surface so

Table 2 Mechanical properties of AA 2198 T3 perpendicular to the rolling direction

UTS (MPa)	YS (MPa)	E (GPa)	Elongation (%)
370	275	–	15

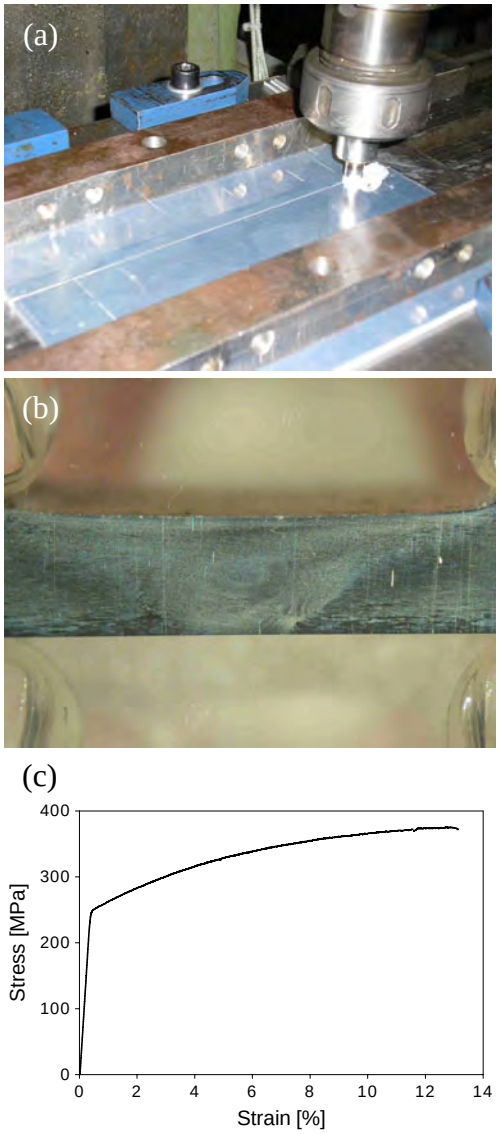

Fig. 1 **a** Configurations of the workpiece, tool and fixture table during the FSW; **b** macro-photography of the FSW joint #1 of Table 6; **c** engineering stress–strain curve for the specimen # 1 of Table 6

attaining the right frictional contact (throughout this and the previous phases, the feed rate of the tool along the vertical axis was set at 5 mm/min and kept constantly at this value);

c) dwelling phase, lasting 4 s, during which the tool, rotating on the same position, softens the material through frictional heating;

d) welding phase, during which the tool is advanced along the joint line and the weld is realized.

To study the dependence of the stationary welding forces (see below) on process parameters a two factors, three levels, design matrix, with the central point replicated four times to estimate variance due to experimental or random variability is adopted. A 3^2 full factorial design results. This design required 9+3 (replications)=12 runs, including the replicated central point. The treatment variables (factors) subjects of this study are the rotational, N (rpm), and welding speed, V (mm/min). Each factor has three levels. The observed responses are the stationary values of the in-plane and forging forces reached during the welding steady state. Trial experiments were preliminarily conducted to determine the working range of the above factors. Feasible limits of the parameters were chosen in such a way that the friction-stir welded joints resulted free from any visible external defects. Macrographs of the welds showed a typical FSW macrostructure consisting of a stir zone (nugget), thermo-mechanically affected zone and heat-affected zone. Figure 1c reports as example the macrograph of the joint #1 of Table 6; the nugget and the onion rings can be easily identified. The chosen experimental design levels of the independent variables are: 500, 700 and 900 rpm for N; 150, 225 and 300 mm/min for V. Figure 2 reports the treatment combination of the above described 3^2 factorial design hereinafter called the FSW force design.

To evaluate the mechanical proprieties of the butt joints, after the welding process, the joints were sliced, as shown in Fig. 3a, using a power hacksaw and then machined to required dimensions as shown in Fig. 3b. Three tensile specimens were fabricated for each joint following the American Society for Testing of Materials (ASTM E8M-04) standards. Hence 12×3=36 specimens were obtained. The tensile tests were carried out at a strain rate of 10^{-4} on a MTS servo-hydraulic testing machine. For each tensile test, the yield strength at 0.2% offset, from now on simply YS (MPa), and the tensile strength (UTS (MPa)) of the welds were determined.

All welds and tests were executed in a randomized order to exclude the disturbing effects of environmental conditions.

Although the specimens were obtained from different positions on the weld, in the analysis of weld mechanical proprieties, this variable is not considered. Indeed, by means of a Nec TH 7800 thermo camera it was checked that heat flux reached a steady-state condition during the FSW as soon as the welding phase starts. In particular, it was checked that the

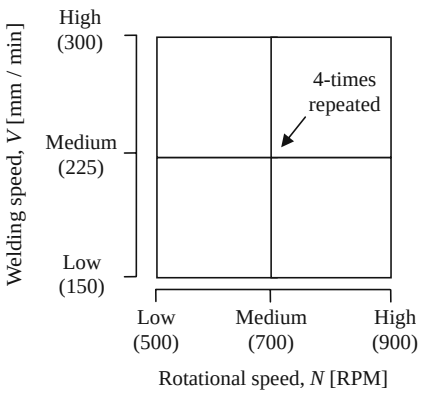

Fig. 2 Treatment combination in the 3^2 FSW force design

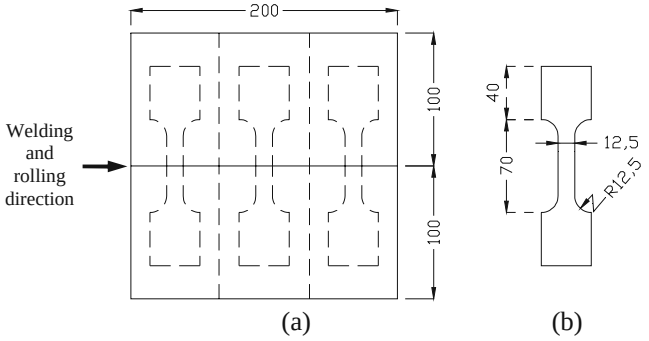

Fig. 3 **a** Scheme of welding with respect to the rolling direction and extraction of tensile specimens and **b** dimensions of tensile specimen according ASTM E8M-04 (all dimensions are in 'mm')

different points along the weld length experience similar temperature history. As a consequence, considering that the amount of the heat conducted into the workpiece dictates the quality and micro-structure of the weld, as well as the residual stress and its mechanical strength, it is possible to conclude that the weld presents the same mechanical proprieties along its length. Subsequently, the 36 tensile tests constitute a 3^2 full factorial design with several repeated points, as it is specified in the followings. In particular, the independent variables are again N and V, characterized by the same previous three design levels, while the observed responses are now YS and UTS of the welds. The treatments combination of this design derives from the one reported in Fig. 2 repeated three times being three the specimens extracted for each combination of rotational and welding speed. As a result, the central point is repeated 12 times, i.e. 4×3 (the four-times repeated central point of the FSW force design in Fig. 2 times the three extracted specimens). From now on, it will be referred to this design as the weld strength design.

3 Results

3.1 Empirical models of the FSW stationary forces

The in-plane and downwards forging forces detected during the welding process have a diagram showing identical features for all the different welding conditions. In Fig. 4, the principal features of the FSW forces-time plot monitored during the run 4, according to the numbering in Table 3 (N=700 rpm, V=150 mm/min), are shown. Figure 4 indicates that the vertical force, Fz, rapidly rises to a first peak value during the insertion of the pin into the material. The pin insertion proceeds with some instability phenomena, revealed by some other peaks followings this first one, and caused by the material being still "cold". Straight afterwards, the frictional heat generated by the pin softens the alloy so that the vertical force undergoes a relaxation from the previous peaks. In the subsequent phase, in particular when the shoulder reaches the material and starts plunging into the surface of the top sheet, the vertical force again increases due to the added frictional work. During the dwelling phase, this steep increase of Fz is once again followed by a reduction of the vertical force due to the plasticization induced into the material by the friction heat. At the beginning of the welding phase, Fz starts rising very rapidly. When the FSW process attains the steady state, the vertical force reaches a stationary value, which is the highest value achieved by Fz in all the different welding conditions investigated. Finally, the vertical force plunges down to zero as the shoulder looses contact with the surface and the pin is extracted from the material. By increasing the tool rotational speed, the height of the different peak decreases. However, Fz gets a stationary value for all the investigated welding conditions; this value is characteristic of the adopted FSW process parameters. On the contrary, the horizontal force, Fx, simply oscillates around zero up to the beginning of the welding phase, when it suddenly reaches a stationary value that keeps until the tool pin extraction. This value is also characteristic of the adopted FSW parameters. The average stationary value of Fx is much lower than the average stationary value of Fz for all the investigated welding conditions. Furthermore, Fx shows a longer steady state than Fz for all the welding conditions under investigation.

Because any set of FSW process parameters has distinctive stationary values of Fx and Fz (from now on called $\overline{Fx}$ and $\overline{Fz}$) reached during the steady state, a

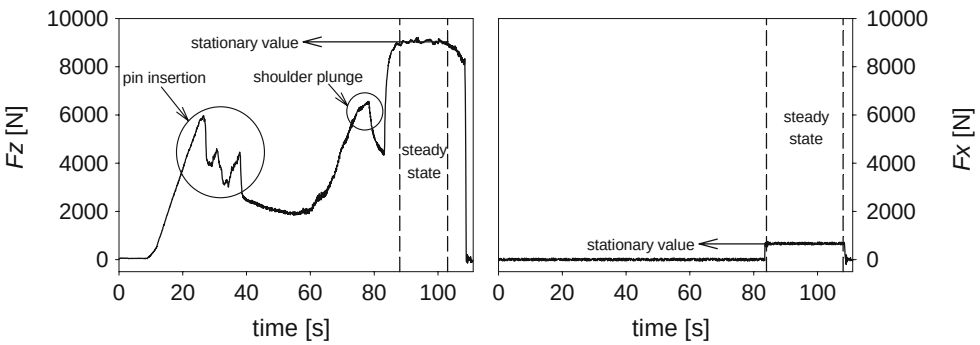

Fig. 4 Run 4 (N=700 RPM, V=150 mm/min), (*right*) variation of in-plane force Fx and (*left*) of the downwards forging force during the welding process

Table 3 FSW force design matrix and experimental results

Run	Factors			
	N (rpm)	V (mm/min)	$\overline{F}x$ (N)	$\overline{F}z$ (N)
1	500	150	9,438	628
2	500	225	10,233	906
3	500	300	10,900	1,217
4	700	150	9,244	664
5	700	225	9,563	877
6	700	225	9,948	857
7	700	225	10,096	884
8	700	225	9,891	878
9	700	300	10,278	1,108
10	900	150	8,004	529
11	900	300	9,635	1,039
12	900	225	8,713	841

empirical model for the welding forces is developed using the FSW force design previously described and displayed in Fig. 2.

The design matrix of the 3^2 factorial design regarding the stationary welding forces and experimental results is reported in Table 3. As before explained, although Table 3 contains ordered data, the design was completely randomized.

A multiple regression model for the stationary FSW forces is proposed using the best subset regression analysis. Mallows' C_P is adopted, in conjunction with the coefficient of determination, R-square (R^2) adjusted R-square (R^2(adj)) and the standard error of the regression (the square root of the mean-square error or root-mean-square error (S)), as the criterion for choosing the best subset of predictors (independent variables) between contending subsets and as a measure of the quality of fit for a model.

As well-known, a model with large R^2 and small number of covariates could be a good choice since large R^2 implies the reliability of fitted values while, in general, a small number of predictors reduces the costs of obtaining information and the costs of process monitoring. In particular, in this paper, R^2 is adopted for an initial screening of the models. However, R^2 has an obvious weakness: it increases as more regressors are added to the model. This often results in overfitting. On the contrary, C_p tends to be less dependent (than R^2) on the number of regressors in the model, and hence, it tends to find the best subset that includes only the important predictors of the respective dependent variable [9, 10]. The general procedure to find an adequate model by means of the C_p statistic is to calculate C_p for all possible combinations of variables and plot the C_p values against p, the Mallow' C_p plot (p is the number of regressors including the constant term) [11]. The model with small C_p value and approximately equal to p is the most "adequate" model. Another criterion for

Table 4 Determination of the best subsets regression for the stationary FSW forces. The best predictor models for FSW forces are highlighted in bold

Vars	R^2	R^2(adj)	C_p	S	N	V	N^2	V^2	$N\,V$
Response is $\overline{F}x$									
1	93.2	92.6	18.1	53.61		X			
1	91.4	90.5	25.2	60.49				X	
2	**98.2**	**97.8**	**0.9**	**29.09**		**X**			**X**
2	98.0	97.6	1.7	30.69		X	X		
3	98.3	97.6	2.7	30.29		X		X	X
3	98.2	97.6	2.8	30.65		X	X		X
4	98.4	97.5	4.0	30.82	X	X	X		X
4	98.3	97.3	4.6	32.24		X	X	X	X
5	98.4	97.2	6.0	33.18	X	X	X	X	X
Response is $\overline{F}z$									
1	48.8	43.7	67.7	574.11			X		
1	46.0	40.6	71.9	589.77	X				
2	93.2	91.6	4.1	221.34			X		X
2	92.9	91.3	4.5	225.71		X	X		
3	**95.7**	**94.1**	**2.3**	**185.14**	**X**	**X**	**X**		
3	94.8	92.8	3.7	205.16	X		X	X	
4	95.9	93.5	4.1	195.33	X	X	X		X
4	95.8	93.5	4.2	195.84	X	X	X	X	
5	95.9	92.6	6.0	208.71	X	X	X	X	X

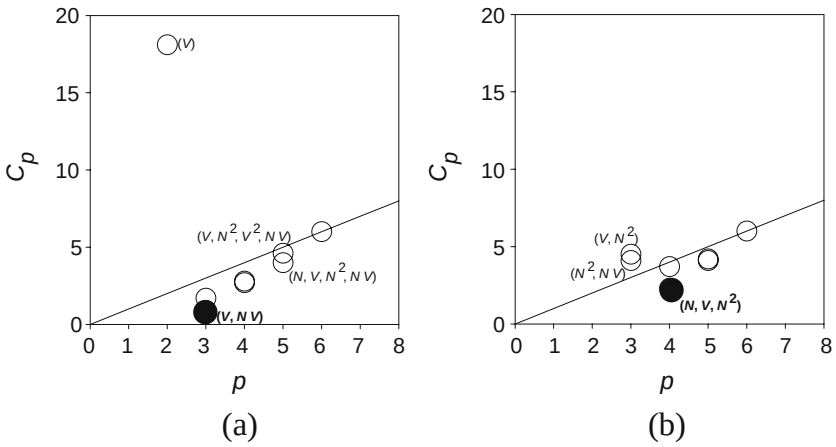

Fig. 5 **a** Mallow' C_p plot for $\overline{F}x$, **b** Mallow' C_p plot for $\overline{F}z$

finding the best possible model is based on the standard error of the regression, *S*. According to this criterion, a model furnishing the lowest *S* and with the fewest predictors might be a sensible model. In this paper, all these statistics are synergically adopted for best subset evaluation.

To obtain the best fit of the data, a non-linear polynomial model for both stationary forces, including second power of the predictor variables (*N* and *V*) and their product (i.e. interaction of predictor variables), is proposed. Hence, the complete list of the five regressor variables used for the model is: *N*, *V*, N^2, V^2, *N V*. There are $2^{\text{predictors}}=2^5=32$ possible models. The regression models are divided in six different sets based on the number of present regressor variables, from zero to five. The number of regression models belonging to each set is given by the binomial coefficient:

$$\begin{pmatrix} \text{regressors} \\ \text{number of regressor variables present in the set (model)} \end{pmatrix}.$$

Set 0, based on zero predictor variables, contains $\binom{5}{0}=1$ model, i.e. $\overline{F}x=\alpha_0+\varepsilon$; set 1, based on one regressor variable, contains $\binom{5}{1}=5$ possible models, e.g.: $\overline{F}x=\alpha_0+\alpha_1 N+\varepsilon$, $\overline{F}x=\alpha_0+\alpha_2 V+\varepsilon$, $\overline{F}x=\alpha_0+\alpha_3 N^2+\varepsilon$, and so on. The FSW force models based on all the regressor variables (set 5 containing one model, the "full model"), are

Table 5 Analysis of variance of the two selected subsets for the FSW process forces

Predictor	Coefficient	SE coefficient	*T*	*P*	
Regression analysis: $\overline{F}x$ versus *V*; *N V*					
Constant	98.23	36.6100	2.68	0.025	
V	4.3191	0.2384	18.11	0.000	
N V	–0.00127	0.0002547	–5.00	0.001	
Source	DF	SS	MS	F	P
Regression	2	417806	208903	246.83	0.000
Residual error	9	7617	846		
Total	11	425423			
Regression analysis: $\overline{F}z$ versus *N*; *V*; N^2					
Constant	5953	1304	4.56	0.002	
N	8.718	3.760	2.32	0.049	
V	9.169	1.008	9.10	0.000	
N^2	–0.00874	0.002672	–3.27	0.011	
Source	DF	SS	MS	*F*	*P*
Regression	3	6168735	2056245	59.99	0.000
Residual error	8	274214	34277		
Total	11	6442949			

Table 6 Weld strength design matrix and experimental results

Run	Factors			
	N (rpm)	*V* (mm/min)	YS (MPa)	UTS (MPa)
1	500	150	248	370
2	500	150	246	368
3	500	150	246	338
4	500	225	252	375
5	500	225	249	289
6	500	225	250	364
7	500	300	252	339
8	500	300	253	360
9	500	300	255	370
10	700	150	247	354
11	700	150	244	355
12	700	150	244	345
13	700	225	254	326
14	700	225	252	343
15	700	225	254	341
16	700	225	252	321
17	700	225	253	302
18	700	225	252	320
19	700	225	254	305
20	700	225	252	306
21	700	225	254	321
22	700	225	254	305
23	700	225	252	263
24	700	225	251	309
25	700	300	252	310
26	700	300	252	312
27	700	300	251	318
28	900	150	246	294
29	900	150	239	295
30	900	150	247	314
31	900	225	245	290
32	900	225	247	260
33	900	225	244	261
34	900	300	248	286
35	900	300	259	292
36	900	300	252	290

written as:

$$\overline{F}x = \alpha_0 + \alpha_1 N + \alpha_2 V + \alpha_3 N^2 + \alpha_4 V^2 + \alpha_5 N \cdot V + \varepsilon$$

and

$$\overline{F}_z = \beta_0 + \beta_1 N + \beta_2 V + \beta_3 N^2 + \beta_4 V^2 + \beta_5 N \cdot V + \varepsilon.$$

In Table 4 the values of the statistics used in the procedure of best subset selection are reported. For every set, one or two models with larger R^2 are shown. In the above-mentioned table, Vars is the numbers of variables in the model; R^2 and R^2(adj) are converted to percentages; predictors that are present in the model are indicated by an *X*. In Fig. 5, for each model and for each stationary force value, the analysis is completed plotting C_p against p, with the line C_p=p added.

Those which are assessed as best predictor models for FSW forces are highlighted in bold in Fig. 5 and in Table 4; in particular, for $\overline{F}x$ the best subset seems the one containing *V* and *N V* as predictor variables and for $\overline{F}z$ it is the one with the predictor variables *N*, *V* and N^2. They are both minimum-C_p subsets showing the maximum R^2(adj) and an acceptable small number of variable amid the regressions under inspection. The fitness of the models is further confirmed by a satisfactory value of determination coefficient, R^2, which is calculated to be 0.982 and 0.957 for $\overline{F}x$ and $\overline{F}z$, respectively, indicating that 98.2% and 95.7 of the variability in the response could be predicted by the models. It is not worth increasing the variable number because this does not cause a significant gain in R^2 (for $\overline{F}x$ the full model shows an R^2 of 0.984 and for $\overline{F}z$ an R^2 of 0.959). Furthermore, their (p, C_p) value is enough close to the line $X = Y$.

The models adequacy is confirmed by the *F* tests reported in Table 5: the analysis of variance shows that the selected regression models are highly significant. Indeed, it is calculated $P<0.001$ with an *F* value of 246.83 [$F_{0.001}(2,9)=16.38$] and $P<0.001$ with an *F* value of 59.99 [$F_{0.001}(3,8)=15.82$] for the $\overline{F}x$ and $\overline{F}z$ regressions, respectively. All the coefficients are evaluated and tested for their significance at 95% confidence level, applying the student's *t* test. The regression coefficients, along with the corresponding *P* values, are shown in the same Table 5.

Then, the final empirical model developed to predict $\overline{F}x$ is given below as:

$$\overline{F}x = 98.23 + 4.32\ V - 0.00127\ N \cdot V,$$

while the force along *z*-axis is regressed as:

$$\overline{F}z = 5,953 + 8.72\ N + 9.17\ V - 0.00874\ N^2.$$

Conformity of the presented models to the assumptions underlying regression analysis (normally and independently distributed errors with mean zero, homoscedasticity of the errors etc.) were checked using classical statistical tools as residual plots, normal probability plots of the residuals etc. Results of these analyses are not reported for the sake of shortness.

It is very interesting to note that both stationary FSW forces depend on the regressor variable *V* and, in particular, they become larger increasing the welding velocity, as it is expected. Besides *V*, $\overline{F}x$ presents only the interaction term between *N* and *V*; this term is present with the minus sign preceding it and a very small coefficient, conferring an

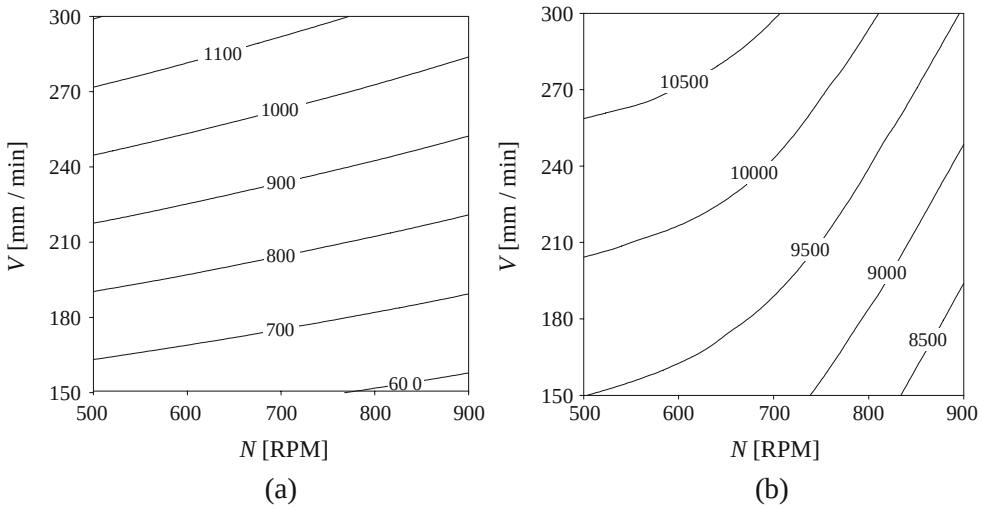

Fig. 6 **a** Contour plot of $\overline{F}x$, **b** contour plot of $\overline{F}z$

extremely slight curvature to the function, which looks like a simple series of almost parallel lines that generally occur with first order models, see the counter plot in Fig. 6a. However, the final effect is that the in-plane force decreases as N rises and grows increasing V. Apart the positive dependence on V, the downwards forging force, $\overline{F}z$, decreases as the rotational speed becomes larger, see Fig. 6b, and this effect is more manifest than for $\overline{F}x$, due to the quite evident curvature conferred to the function by the presence of the N^2 term; this curvature is especially evident at high values of V and low values of N. However, as it has been already experimentally observed [3, 4, 12], the welding speed has little effect on the FSW forces, while increasing the rotational speed causes a significant decrease of their stationary values. Obviously, this is determined by the greater heat production resulting from the higher rotational speed. In conclusion, $\overline{F}x$ and $\overline{F}z$ are characterized by a simple and analogous dependence upon N and V: basically, they strongly decrease increasing N, and slightly increase with V.

Table 7 Determination of the best subsets regression for YS and UTS. The best predictor models for YS and UTS are highlighted in bold

Vars	R^2	R^2(adj)	C_p	S	N	V	N^2	V^2	$N\,V$
Response is YS									
1	42.7	41.0	13.5	3.13		X			
1	38.0	36.2	17.2	3.26				X	
2	52.9	50.1	7.4	2.88			X		X
2	50.3	47.3	9.4	2.96		X		X	
3	**58.5**	**54.6**	**4.9**	**2.75**	**X**		**X**		**X**
3	58.3	54.3	5.1	2.75	X	X	X		
4	61.5	56.5	4.6	2.69	X	X	X	X	
4	59.1	53.8	6.5	2.77		X	X	X	X
5	62.2	55.9	6.0	2.71	X	X	X	X	X
Response is UTS									
1	53.6	52.2	8.7	22.23	X				
1	53.1	51.7	9.1	22.35			X		
2	58.7	56.2	6.1	21.28				X	X
2	57.5	54.9	7.2	21.59	X				X
3	**65.5**	**62.3**	**2.2**	**19.75**		**X**	**X**	**X**	
3	64.6	61.3	3.0	20.00	X	X		X	
4	65.6	61.2	4.1	20.04		X	X	X	X
4	65.6	61.1	4.2	20.05	X	X	X	X	
5	65.8	60.0	6.0	20.33	X	X	X	X	X

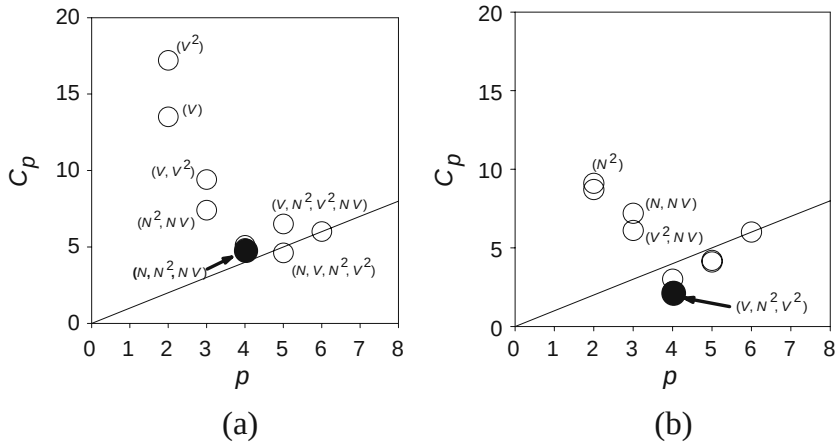

Fig. 7 **a** Mallow' C_p plot for YS, (**b**) Mallow' C_p plot for UTS

3.2 Empirical models of the mechanical strength of the welds

The weld strength design matrix and experimental results of the 36 tensile tests are reported in Table 6. Figure 1c reports as example the engineering stress–strain curve for the specimen #1 of Table 6.

A second order polynomial model is proposed for YS and UTS as function of N and V. Again, YS and UTS regression analyses are tested against the following regression variables: N, V, N^2, V^2, $N\,V$. The best subset of terms to be included in the model is defined using Mallows' C_P in conjunction with R^2, R^2(adj) and S. Table 7 contains the results obtained for the determination of the best subsets regression. As done before, for each number of terms included in the model under investigation the two models individuated by larger R^2 are displayed. Figure 7a, b reports the Mallow' C_p plots for YS and UTS. The models assessed as best are highlighted (in bold) in Table 7 and Fig. 7.

For YS, (N, N^2, $N\,V$) is selected as best regression subset. Although, the (N, V, N^2, V^2) subset shows a lower C_p, it is rejected due to its larger number of regression variables. Indeed, it is worthless to adopt a more complicated four-variable model when, swapping the three-variable model for the four-variable one, a little profit is realized in terms of S; specifically, S passes from 2.75 to 2.69. Moreover, the chosen model has a good C_p and a fairly excellent R-Sq(adj), compared to the other models.

From the elaboration of UTS data, the regression model containing the terms V, N^2, V^2 is picked out. Maximizing the adjusted determination coefficients and minimizing S,

Table 8 Analysis of variance of the two selected subsets for the mechanical proprieties of the welds

Predictor	Coef	SE Coef	T	P	
Regression analysis: YS versus N, N^2, $N\,V$					
Constant	224.69	11.02	20.38	0.000	
V	0.0672	0.03238	2.08	0.046	
N^2	−0.00006389	0.00002293	−2.79	0.009	
$N\,V$	0.00006925	0.00001203	5.76	0.000	
Source	DF	SS	MS	F	P
Regression	3	341.63	113.88	15.04	0.000
Residual error	32	242.26	7.57		
Total	35	583.89			
Regression analysis: UTS versus V, N^2, V^2					
Constant	564.89	58.71	9.62	0.000	
V	−1.6131	0.5308	−3.04	0.005	
N^2	−0.00011768	0.00001656	−7.11	0.000	
V^2	0.003328	0.001172	2.84	0.008	
Source	DF	SS	MS	F	P
Regression	3	23,721.0	7,907.0	20.25	0.000
Residual Error	32	12,493.2	390.4		
Total	35	36,214.1			

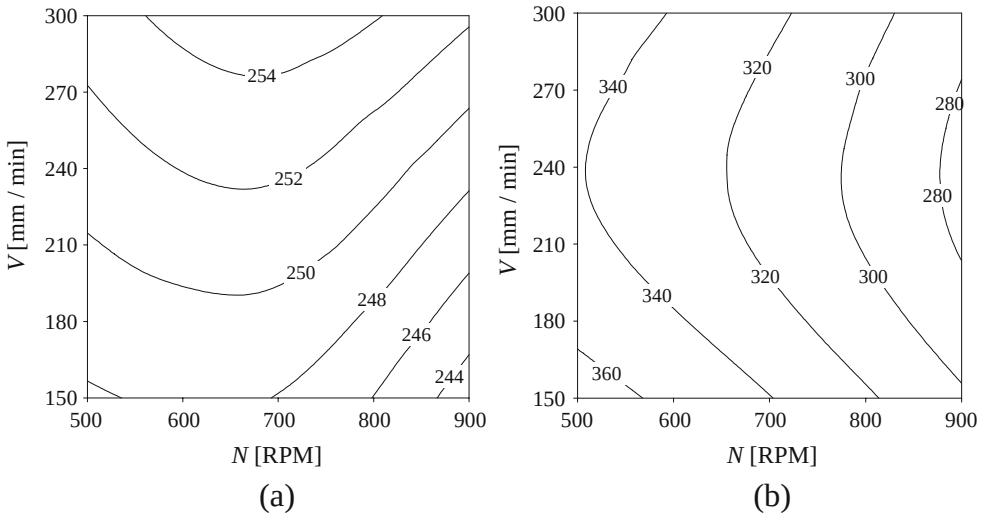

Fig. 8 **a** Contour plot of YS, **b** contour plot of UTS

this combination is distinctly recognized as the best subset. Moreover, the model contains a fairly low number of terms, so avoiding redundant information.

The analyses of variance of the models adopted for YS and UTS, in Table 8, confirm the correctness of the subsets. The analyses show that these regression models are highly significant: $P<0.001$ with F value of 15.04 and $P<0.001$ with F value of 20.25 for YS and UTS regressions, respectively [$F_{0.001}(3, 32)=6.93$]. All the evaluated coefficients pass the t test used to check their significance at 95% confidence level. The regression coefficients, along with the corresponding P values, are shown in the same Table 8.

Then, the final empirical models developed to predict YS and UTS are:

$$\mathrm{YS} = 224.69 + 0.0672 \cdot N - 0.000064 \cdot N^2 + 0.000069 \cdot N \cdot V,$$
$$\mathrm{UTS} = 564.89 - 1.6131 \cdot V - 0.00011768 \cdot N^2 + 0.003328 \cdot V^2.$$

YS depends on N and N^2. The interaction term between N and V is also present as the elliptical contours clearly indicate [13], see Fig. 8a. It is possible to conclude, by examining the contour plot in Fig. 8a, that YS is a little more sensitive to changes in welding speed than to changes in rotational speed. UTS is a function of V and V^2; furthermore, it also depends on N^2. Indeed, Fig. 8b exhibits almost circular contours, surely more circular than YS, which suggest a larger independence of factor effects, namely N and V. Finally, UTS seems more sensitive to changes in N than to changes in V, as it is evident from Fig. 8b.

The contour plots shown in Fig. 8 clearly bring out a more complex behaviour of YS and UTS, compared to the welding forces, which simply increase with V and decrease with N. In particular, the optimum YS is exhibited for values of N at the middle of the working range, around 680/700 rpm, and for high values of V, about 300 mm/min, while, the optimum UTS is obtained at medium values of V, nearly 240 mm/min, and high values of N, around 900 rpm.

Table 9 Result of the multiresponse optimization

Optimum value=0.8404				
Factor	Response	Low	High	Optimum
N		500	900	531
V		150	300	300
	UTS			348
	YS			253

3.3 Optimising FSW parameters to maximise YS and UTS

To maximize the weld mechanical strength, i.e. to optimize both YS and UTS, on which the quality of a weldment is based, it is essential to select and control the

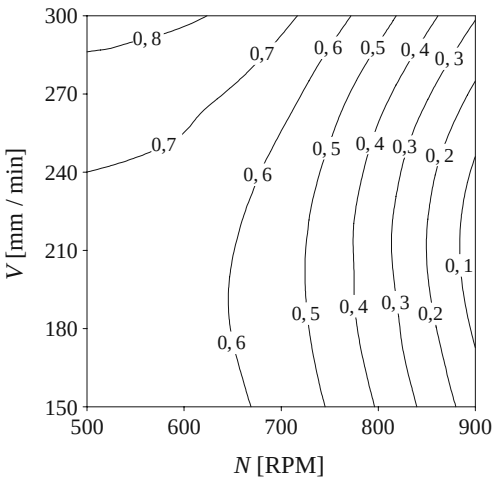

Fig. 9 Contour plot of the overall desirability function for the levels of rotational and welding speeds

welding process parameters, N and V. However, the previous analysis showed that the welding process parameters for which it is possible to achieve the maximum UTS do not match with those maximizing the YS. A typical multiresponse optimization problem, involving conflicting responses, arises. In this paper, a simultaneous optimization technique, based on the desirability function (DF) [14, 15] is used to optimize the multiple responses, YS and UTS. In particular, the DF approach is used to find the best compromise between the two responses, based on the empirical equations above established for YS and UTS.

The DF approach transforms an estimated response (e.g., the ith estimated response $\widehat{y}_i$) into a scale-free value, called desirability function, denoted as d_i for $\widehat{y}_i$, $d_i(\widehat{y}_i)$. It is a value between 0 and 1, increasing as the corresponding response value becomes more desirable. If the response is to be maximized, as in this case, the individual desirability is generally defined as

$$d_i(\widehat{y}_i) = \begin{cases} 0 & \text{if } \widehat{y}_i < L_i \\ \frac{\widehat{y}_i - L_i}{U_i - L_i} & \text{if } L_i \le \widehat{y}_i \le U_i \\ 1 & \text{if } \widehat{y}_i > U_i \end{cases},$$

where L_i and U_i are the lower and upper values, respectively, for response $\widehat{y}_i$. The overall desirability D, another value between 0 and 1, is defined by the weighted geometric mean of the individual desirability values (i.e., d_i's):

$$D = d_1^{w_1} \times d_2^{w_2} \times d_3^{w_3} ....., \; 0 < w_i < 1 \text{ and } w_1 + w_2 + w_3 + ... = 1,$$

where w_i is the relative importance assigned to the response i. The relative importance is a comparative scale for weighting each of the resulting d_i in the overall desirability product. It is noteworthy that the outcome of the overall desirability D depends on the w_i value, which offers users flexibility in the definition of desirability functions. The optimal setting is determined by maximizing D, being evident that D will increase when the balance of the properties becomes more favourable.

In this study, the responses, YS and UTS, are transformed into appropriate desirability scales d_1 and d_2 according to the following equations:

$$d_1 = \begin{cases} 0 & \text{if YS} < \text{YS}_{\text{min}} \\ \frac{\text{YS} - \text{YS}_{\text{min}}}{\text{YS}_{\text{max}} - \text{YS}_{\text{min}}} & \text{if YS}_{\text{min}} \le \text{YS} \le \text{YS}_{\text{max}} \\ 1 & \text{if YS} > \text{YS}_{\text{max}} \end{cases},$$

$$d_2 = \begin{cases} 0 & \text{if UTS} < \text{UTS}_{\text{min}} \\ \frac{\text{UTS} - \text{UTS}_{\text{min}}}{\text{UTS}_{\text{max}} - \text{UTS}_{\text{min}}} & \text{if UTS}_{\text{min}} \le \text{UTS} \le \text{UTS}_{\text{max}} \\ 1 & \text{if UTS} > \text{UTS}_{\text{max}} \end{cases},$$

where YS_{max}, YS_{min} and UTS_{max}, UTS_{min} are calculated by means of the preceding regression equations.

Clearly, d_1 and d_2 increase as long as YS and UTS increase. The overall desirability D was calculated by

$$D = d_1 \times d_2,$$

because the same importance is attributed to the different responses, namely $w_1 = w_2 = 1$.

The results of the optimization are reported in Table 9, where the maximum global desirability function (D= 0.8404), the best achievable of each of the responses, YS and UTS, and the optimal welding parameters, N and V, are presented. In addition, the optimization results are also illustrated with the contour plots of D, in Fig. 9.

The optimal result is obtained at N=531 rpm and V= 300 mm/min, which correspond to UTS=348 MPa and YS=253 MPa. At this operating condition, the empirical models previously developed for the FSW forces predict that the stationary welding forces are: $\overline{F}x = 1{,}191\,\text{N}$ and $\overline{F}z = 15{,}798\,\text{N}$.

4 Conclusion

- Two sets of empirical models, containing rotational and welding speeds as independent variables, are developed at 95% confidence level. The first one predicts the in-plane and downward forging forces in the FSW of AA 2198 butt joints. The second one predicts the yield and tensile strengths of the friction stir welded AA 2198 butt joints. The models are developed using statistical tools such as design of experiments and regression analysis. The choice of the predictive variables to be included in the model is carried out by means of the Mallows' Cp. in conjunction with R^2, R^2(adj) and the standard error of the regression.
- Contour plots are drawn to study the interaction effect of the welding parameters under study on FSW forces and mechanical strength of friction stir welded joints of the AA 2198 aluminium alloy. Welding forces demonstrate a simple and analogous dependence upon process parameters under concern: they decrease increasing the rotational speed and slightly rise with the welding speed, however following dissimilar laws. On the contrary, yield and tensile strengths show a very different dependence on rotational and welding speeds. In particular, they reach their maximum for different and incompatible values of the process parameter under study.
- The desirability function approach is used for simultaneous optimization of yield and tensile strengths of the friction stir welded AA 2198 butt joints. The multi-objective optimization methods indicates that best quality joints can be manufactured by using the optimal conditions of 531 rpm and

300 mm/min for rotational and welding speed, respectively, namely realizing the FSW in the so-called cold condition.

- The method developed in this work may provide an attractive solution to simultaneous optimization of several response variables, allowing high performance production. The results are expected to be helpful in optimizing the FSW process and in facilitating its automation to ensure good weld quality.

References

1. Thomas WM (1991) Friction stir welding, international patent application no. PCT/GB92/02203 and GB Patent Application No. 9125978.8, December, US Patent No. 5,460,317
2. Cavaliere P, De Santis A, Panella F, Squillace A (2009) A effect of anisotropy on fatigue properties of 2198 Al–Li plates joined by friction stir welding. Eng Fail Anal 16:1856–1865
3. Chen C, Kovacevic R (2004) Thermomechanical modelling and force analysis of friction stir welding by the finite element method. J Mech Eng Sci C 218:509–519
4. Prisco A, Acerra F, Squillace A, Giorleo G, Pirozzi C, Prisco U, Bellucci F (2008) LBW of similar and dissimilar skin-stringer joints. Part I: process optimization and mechanical characterization. Adv Mater Res 38:306–319
5. Elangovan K, Balasubramanian V, Babu S (2009) Predicting tensile strength of friction stir welded AA6061 aluminium alloy joints by a empirical model. Mater Des 30:188–193
6. Elangovan K, Balasubramanian V, Babu S, Balasubramanian M (2008) Optimising friction stir welding parameters to maximise tensile strength of AA6061 aluminium alloy joints. Int J Manuf Res 3:321–334
7. Balasubramanian V (2008) Relationship between base metal properties and friction stir welding process parameters. Mater Sci Eng A 480:397–403
8. Lakshminarayanan AK, Balasubramanian V (2009) Comparison of RSM with ANN in predicting tensile strength of friction stir welded AA7039 aluminium alloy joints. Trans Nonferr Met Soc China 19:9–18
9. Hocking RR, Leslie RN (1967) Selection of the best subset in regression analysis. Technometrics 9:531–540
10. Mallows CL (1973) Some comments on C_p. Technometrics 15:661–675
11. Mallows CL (1995) More comments on C_p. Technometrics 37:362–372
12. Balasubramanian N, Gattu B, Mishra RS (2009) Process forces during friction stir welding of aluminium alloys. Sci Technol Weld Join 14:141–145
13. Montgomery DC (2001) Design and analysis of experiments. Wiley, New York
14. Harrington E Jr (1965) The desirability function. Industr Qual Control 21:494–498
15. Derringer G, Suich R (1980) Simultaneous optimization of several response variables. J Qual Technol 12:214–219